Acta Crystallographica Section D
Biological Crystallography
ISSN 0907-4449

Experimental evidence for the stability of the depletion zone around a growing protein crystal under microgravity

Fermín Otálora,[a] María Luisa Novella,[a] José Antonio Gavira,[a] Bill R. Thomas[b,c] and Juan Manuel García Ruiz[a]*

[a]Laboratorio de Estudios Cristalográficos, IACT, CSIC-Universidad de Granada, Campus Fuentenueva, 18002-Granada, Spain, [b]Universities Space Research Association, 4950 Corporate Drive, Suite 100, Huntsville, AL 35806, USA, and [c]Center for Microgravity Materials Research, University of Alabama in Huntsville, Huntsville, AL 35899. USA

Correspondence e-mail: jmgruiz@ugr.es

Received 25 July 2000
Accepted 5 January 2001

Experimental evidence is presented for the first time for the development and time evolution of concentration-depletion zones around protein crystals growing in microgravity and gelled on-ground experiments. Crystal motion and buoyancy-driven fluid movements as a result of residual accelerations and *g*-jitters are demonstrated to have an adverse effect on the stability of these depletion zones, provoking the breakdown of their radial symmetry. These findings may explain some of the controversial results reported on the quality of single crystals grown under microgravity in previous space missions.

1. Introduction

Crystal growth under microgravity proceeds by the same chemical processes as on ground, the only difference between them being fluid dynamics: mass transport is nominally diffusive in the weightless environment. Understanding crystal quality enhancement in microgravity crystal growth is therefore a problem mainly related to fluid physics.

Zero-gravity environments do not exist in the real world; all facilities for microgravity experimentation suffer from some degree of residual acceleration and *g*-jitters, arising mostly from orbiter manoeuvres. The influence of these *g*-jitters on the dynamics of protein crystal growth in microgravity has been observed recently (García-Ruiz & Otálora, 1997; Snell *et al.*, 1997; García-Ruiz *et al.*, 2001). These deviations from true microgravity are known to be the origin of a convective contribution to mass transport triggered by surface tension at free fluid interfaces or by density gradients over the fluid (Walter, 1987). Free fluid interfaces do exist in some protein crystal growth techniques, namely in all variations of vapour-transport methods. For these experiments, surface-tension driven Marangoni convection is known to occur even in microgravity scenarios (Molenkamp *et al.*, 1994; Savino & Monti, 1996). Crystal movements consistent with this instability have been described in microgravity protein crystal growth experiments (Chayen *et al.*, 1997). The use of crystallization techniques without liquid–gas surfaces, such as free interface diffusion, under microgravity is in principle a good candidate for growing crystals in a convection-free scenario. Even in this case, however, the effect of buoyancy-driven convection must be assessed because concentration (density) gradients exist in the crystallizing solutions as an intrinsic consequence of the very crystal-growth process.

As a crystal grows from the solution, it depletes the concentration of the growth units that are incorporated into the crystal lattice producing a concentration-depleted zone (CDZ) around it. In this region, the solute concentration changes continuously from the concentration at the crystal

face to the concentration in the bulk of the solution. The concentration profile in the CDZ varies with time as the crystal grows and is controlled by the balance between the flow of growth units towards the crystal face and the rate of incorporation of these growth units into the crystal lattice. The kinetics of incorporation at the crystal surface are linked to the bond configuration of the crystallographic structure, while the flow towards the crystal face is highly dependent on the mass-transport properties in the bulk solution, which turn out to be crucial for the overall crystal-growth process. The diffusive transport through the depletion zone around a growing crystal is therefore responsible for any observable difference between on-ground and microgravity experiments including crystal quality enhancement.

CDZs have been a topic of interest for protein crystal-growth scientists since the first works in this field (Kam *et al.*, 1978). More recently, the availability of suitable interferometric facilities has renewed this interest. Recent literature includes studies of small-molecule crystal growth on ground and in microgravity (Tsukamoto *et al.*, 1998; Maruyama *et al.*, 1999) and of macromolecule crystal growth on ground (Komatsu *et al.*, 1993; Miyashita *et al.*, 1994; McPherson *et al.*, 1999). In all cases, the experimental setup includes a Mach–Zehnder interferometer alone or in combination with a Michelson interferometer to record the growth of crystal faces. Mach–Zehnder interferometry was used in the experiments here reported to monitor the mass-tranport dynamics in the fluid phase in microgravity. Residual accelerations and *g*-jitters can produce both crystal movements (García-Ruiz & Otálora, 1997; Riès-Kautt *et al.*, 1997; Snell *et al.*, 1997; Boggon *et al.*, 1998) and fluid flow. Crystal movement can in turn produce fluid movement by stirring the solution and fluid flow can produce crystal movement by dragging. To understand the dynamics of CDZs the effects of fluid and crystal movements must be separated. We present in this paper the first results from microgravity-conducted experiments designed to monitor for the first time the development of the depletion zone around protein crystals and observing separately crystal and fluid motion. These experiments were the following.

Experiment 1. In order to be able to study quantitatively any distortion of the depletion zone as a consequence of crystal movements, we had to maximize the ratio between the crystal velocity and the bulk diffusion coefficient. This was the rationale for the selection of a large protein (horse spleen ferritin) having a small diffusion constant owing to its large molecular size, being 12 nm in diameter (Hempstead *et al.*, 1997), and producing crystals of relatively high density owing to their iron core (about 112 kDa iron in a macromolecule of 474 kDa). Ferritin was used to perform a free interface diffusion experiment monitored with interferometry, with the objective of following the movement of crystals surrounded by their CDZ.

Experiment 2. To observe the effect of fluid motion without crystal movement, a seeding experiment was designed in which a large gel-reinforced (García-Ruiz *et al.*, 1998) lysozyme seed crystal was glued to one of the walls of the reactor and the initial conditions were selected in such a way that no additional nucleation occurred during the experiment, so a large depletion zone would develop and evolve. Growing a seed without further nucleation during a preprogrammed flight experiment pushed to the limits the requirements of this experiment. Many preliminary tests and computer simulations led us to the selection of hen egg-white lysozyme as the protein to crystallize, because its solubility curve is perfectly known (definitely a must for designing this demanding experiment) and because of our experience in producing silica gel reinforced crystals to be used as seeds. Solubility data used in the preparation of this experiment were obtained by fitting data gathered from different papers in the literature (see Otálora & García-Ruiz, 1997, for details). This experiment was performed both on-ground and in microgravity and monitored using interferometry.

2. Material and methods

The experiments were performed in the Advanced Protein Crystallization Facility (APCF; Bosch *et al.*, 1992) during the STS-95 mission. Free interface diffusion (FID) reactors were selected to avoid free fluid interfaces. Fig. 1 shows the geometry of the reactors used. Protein and precipitating agent solutions are in the respective reservoirs and are initially separated by a rotatory plug. This plug contains a channel that is filled with the desired solution (usually precipitating agent or buffer). Once in microgravity conditions, this plug is rotated so that it now sets in contact the protein and precipitating agent solutions, activating the experiment. The reverse rotation of the plug is used to deactivate the reactor.

For experiment 1, ferritin solutions were prepared from purified monomeric concentrated solutions. The concentration

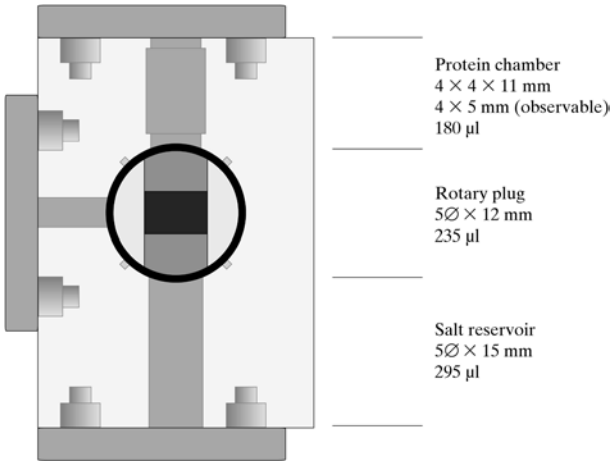

Figure 1
Schematic representation of the APCF reactors used for the experiments. The salt reservoir (bottom) and the protein chamber (top) are set in contact when in orbit by turning the rotatory plug. The size and volume of each relevant chamber are indicated. The reactor body is made of transparent fused silica and its walls are flat enough to allow interferometric data collection. The observation window for the interferometer covers the central part of the protein chamber.

of the solution filling the protein chamber was set to 18 mg ml^{-1}. The rotatory plug was filled with a gelled [1%(*w*/*v*) agarose] solution containing 3%(*w*/*v*) cadmium sulfate (Sigma analytical grade). Finally, the salt reservoir contained a 3%(*w*/*v*) solution of cadmium sulfate. The three solutions were buffered to pH 5.0 using 0.2 *M* sodium acetate. Initial conditions were selected to optimize the nucleation flux (number of crystals nucleated per unit volume and time), our aim being to obtain a number of crystals that was low enough to track their movements.

For experiment 2, 100 mg ml^{-1} solutions of lysozyme (Seikagaku E98301) containing 1.2%(*w*/*v*) sodium chloride (Sigma analytical grade) were used in the protein chamber. The salt was added to reduce the local salt concentration gradient at the entry of the protein chamber; this helps in reducing the risk of homogeneous nucleation. In order to avoid convective transport in the on-ground experiment, 0.1%(*w*/*v*) agarose was added to the lysozyme solution, which makes the solution behave as a high-viscosity non-Newtonian fluid. No agarose was added in the microgravity experiment. The rotatory plug was filled with a gelled [0.5%(*w*/*v*) agarose] 1.25%(*w*/*v*) solution of sodium chloride and the salt reservoir was filled with an ungelled 3.25%(*w*/*v*) solution of sodium chloride. The three solutions were buffered to pH 4.5 using 0.5 *M* sodium acetate buffer. The selection of the initial conditions was based on the demanding requirements of this experiment: during the equilibration of the protein chamber, the concentration must at all times remain within the metastable zone, allowing the growth of the seed but avoiding further nucleation that would spoil the interferometry images. The equilibration pathways through the solubility diagram were carefully studied using both computer simulation and on-ground test experiments. As the objective of this experiment was the observation of a large depletion zone around a stationary crystal, a seed crystal was attached to the wall of the protein chamber. Large seed crystals (up to 16 mm^3 in volume) were grown in high-concentration silica gels. This growth technique is known to produce 'reinforced' crystals that can be easily handled and can even be glued to rigid substrates (García-Ruiz *et al.*, 1998). After performing vibration tests of the APCF with the flight reactors mounted containing these seeds, we decided to use 2 × 1.5 × 1.5 mm (4.5 mm^3) seeds grown in silica gels [5%(*w*/*v*) tetramethoxysilane] and to fix them using Loctite Super Glue-3 directly on the reactor wall.

The APCF Mach–Zehnder interferometer powered by a 850 nm laser diode was used to collect interferograms from various reactors in microgravity following a programmed data-acquisition sequence (a descripton of this interferometer can be found in Snell *et al.*, 1996). A pseudo-phase-shifting method was used to improve the accuracy of the phase images. This method consists of imposing a small angle between the wavefronts of the sample and reference beams so that the 'white' image (before activation of the reactor) already has a number of parallel fringes. Measurement of fringe deviation in a small refractive-index gradient is then more accurate than the measurement of small changes in gray value. For the on-ground seeding experiment, a HeNe (632 nm wavelength) Mach–Zehnder interferometer installed in our laboratory was used. No pseudo-phase-shifting technique was used in this case as the instrument was operated in a dedicated mode (instead of time-shared as in the APCF) and the number of interferograms collected could be optimized to obtain an adequate tracking of the interference fringes. The evaluation of interferograms was performed in the following way: every interferogram was transformed to a phase image by fringe counting at each point in a dense array evenly distributed over the image. Real phase values were obtained by subtracting the reference phase field (the one computed from the reference 'white' interferogram before activation) from each phase map. Phase-difference maps were transformed to concentration-difference maps using concentration *versus* refractive index

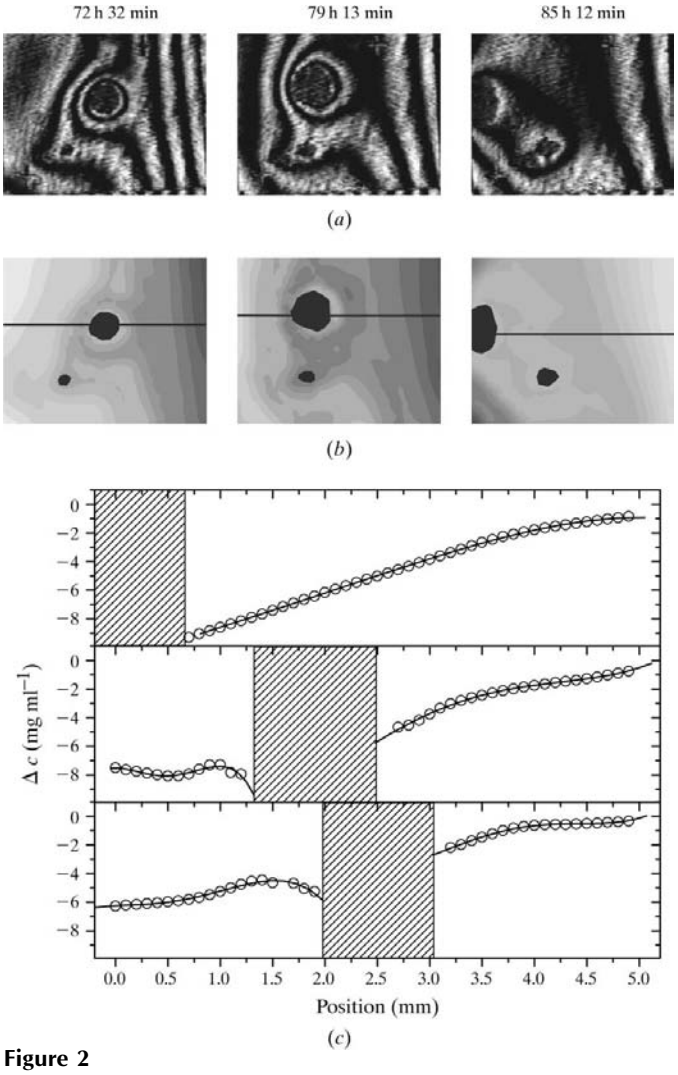

Figure 2
Time series of three consecutive interferograms collected from experiment 1. The top row (below time labels indicating the elapsed experiment time) contains the interferometric images as obtained in microgravity. The middle row contains the concentration maps computed from these interferograms, along with the crystals' outline and a horizontal line indicating the position of the concentration profiles shown in the bottom plot. Dashed zones in the plots correspond to the crystal position at each time.

calibration curves previously obtained in our laboratory by refractometry. Calibration curves for 850 nm were extrapolated using the Cauchy formula.

3. Results and discussion

The top row of Fig. 2 shows three consecutive interferograms (time indicated at the top of each column) collected from experiment 1. At the time at which these interferograms were obtained, during the third day after reactor activation, the protein chamber was almost homogeneized, *i.e.* the concentration of cadmium sulfate was almost equal over the protein chamber and the pattern of fringes was only related to the concentration of protein. The overall gradient observed in the interferograms is a consequence of the growth of a large number of crystals to the left of the image (at the limit between the rotatory plug and the protein chamber). Two crystals can be observed in the 5 × 4 mm field of view; the small crystal located in the lower part of the image is attached to the wall of the reactor and consequently cannot move, while the largest crystal in the centre is floating in the solution and moves across the field of view. The average rate of motion of the largest crystal between the first and second images was $R_{12} = 104\ \mu m\ h^{-1}$ and between the second and third images was $R_{23} = 256\ \mu m\ h^{-1}$. The middle row of Fig. 2 shows the concentration fields reconstructed from the interferogram and the bottom row shows sections of this concentration field along the horizontal lines indicated in the middle-row plots. As the crystal moves, the depletion zone around the large crystal changes from slightly deformed in the left interferogram to severely distorted in the middle to almost nonexistent in the right interferogram.

The microgravity environment during the STS-95 mission was very noisy, with a relatively high level of residual acceleration and periods of large acceleration events (*g*-jitters) at least three times during the mission. This choppy history was recorded by the accelerometers on board (SAMS-FF facility) and their effects on other experiments performed during this mission have been reported (García-Ruiz *et al.*, 2001). On the microscopic scale, these *g* fluctuations have been reported as a possible cause of fluctuations of the growing interface and modifications of the interfacial growth mode (Wang *et al.*, 1999). On a larger scale, the relatively fast crystal movements observed in Fig. 2 (induced by these large *g*-jitters) do break the symmetry of the depletion zone around the growing crystal as expected whenever the velocity of flow of macromolecules towards the crystal face is slower than the rate of motion of the crystals (García-Ruiz, 1999). The flow rate of solute molecules towards the crystal face is characterized by a kinetic coefficient, $k_D = D/l$, where D is the diffusivity of the solute and l is the thickness of the depletion zone. For the experiment analysed, the thickness of the depletion zone is between 1 and 1.4 mm and the diffusivity of the ferritin is $D = 3.2 \times 10^{-7}\ cm^2\ s^{-1}$ (Petsev *et al.*, 2000). From these values, we calculated the flow velocity: it varies between $k_{12} = 115\ \mu m\ h^{-1}$ (for $R_{12} = 104\ \mu m\ h^{-1}$) and $k_{23} = 82\ \mu m\ h^{-1}$ (for $R_{23} = 256\ \mu m\ h^{-1}$). Therefore, the velocity of the flow will be approximately the same as the rate of motion of the crystals in the first case and smaller than the rate of motion in the second one. As a consequence, we must observe some modification of the depletion zone in the first case and an appreciable alteration in the second one, as confirmed by the interferograms.

Would these accelerations also modify the CDZs around fix growing crystals? The target of experiment 2 was to answer this question. Fig. 3 shows two interferograms collected at approximately the same time in the microgravity (right) and on-ground (left) seeding experiments. As in Fig. 2, the middle row shows the concentration fields reconstructed from the

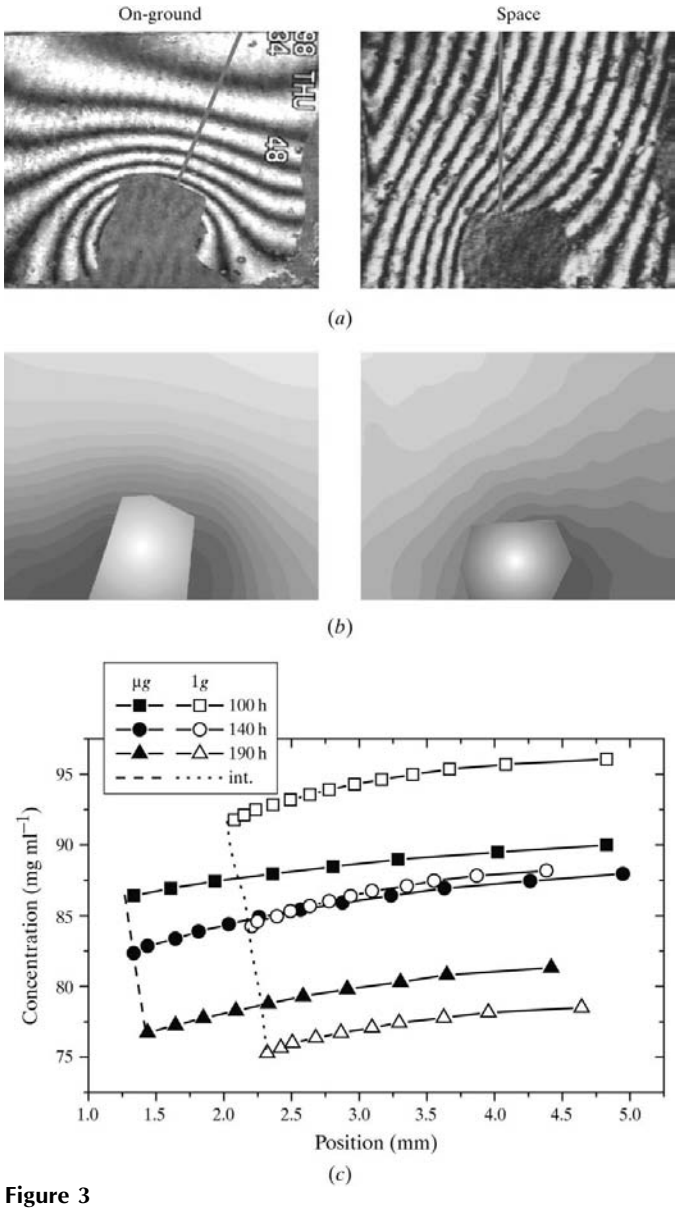

Figure 3
Representative interferograms from experiment 2. The left column corresponds to the on-ground experiment and contains the actual interferogram (top) and the concentration map (middle). The same information is presented on the right for the microgravity experiment at aproximately the same time. Three concentration profiles along the perpendicular to the face indicated in the concentration map are shown in the plot at the bottom for both on-ground and space experiments.

interferograms and the bottom row shows some concentration profiles along perpendiculars to crystal faces (indicated in the top row). Both experiments in APCF reactors clearly show the depletion zone around the growing seed. The curved interference fringes are more evident in the on-ground experiment because a pseudo-phase-shift technique was used in microgravity, which masks the fringes. At first sight, it is clear that the CDZ is more distorted around the seed grown in microgravity than in the on-ground gelled experiment. This contraintuitive result can be easily understood by simple order-of-magnitude theoretical considerations: gravity acceleration was on average 10^5 times higher in the on-ground experiment, but the characteristic size of the system was 10^4 times smaller (gel pore size; Pernodet *et al.*, 1997) so the Grashof number for the on-ground experiments was 10^6 times smaller for the gelled on-ground experiment than for the microgravity experiment. The Grashof number measures the ratio between buoyancy and viscous forces; for a given experimental setup, larger values for this number mean larger buoyancy forces and therefore a larger convective contribution. For the two experiments reported here, it is clear that the balance between buoyancy and viscous forces was more favourable in the gelled on-ground experiment; therefore, the contribution of buoyancy-driven convection was more important in the space experiment.

Owing to the more diffusive environment in the gelled on-ground experiment, both the supersaturation and supersaturation rate at the surface of the growing seed were higher in the gelled on-ground experiment than in space. Supersaturation at the surface of the crystal varied during the experiment from 3.5 to 4.8 on ground and from 3.6 to 4.1 in microgravity; the average supersaturation rate was 0.203 h^{-1} for the on ground and 0.121 h^{-1} for the microgravity experiment. The growth rate of the seed was consequently also higher on ground than in the microgravity experiment (Fig. 4*a*). These growth curves were fitted to power laws with exponents closer to 1 than to 0.5 in both cases, but higher in the microgravity experiment (0.94 compared with 0.89). This deviation from diffusion-controlled growth, which would show a square-root dependence of the crystal size on time, illustrates the fact that even when diffusive transport is ensured, no guarantee exists that the crystal will grow in the diffusion-controlled regime: the growth regime is a function of the ratio between diffusion transport and surface-attachment kinetics (Chernov, 1984). Seed growth also starts later (113.8 h) in microgravity than in the gelled on-ground experiment (50.4 h); this time indicates the transition from the equilibrium to the supersaturated conditions as a consequence of the salt diffusion and is consistent with some degree of density stratification in the space experiment owing to buoyancy. The concentration gradients at the surface of the seed show a similar time evolution (Fig. 4*b*), increasing at first owing to the creation and development of the depletion zone as the crystal starts growing and then decreasing owing to the relaxation of the diffusive gradient. Unfortunately, the size of the growth chamber (4 mm) is not large enough to allow the depletion zone to reach steady state. Both overall and local concentration gradients were higher in the on-ground than in the microgravity experiment. The kinetic implications of these observations on the CDZ gradient at the crystal–liquid interface will be discused elsewhere.

4. Conclusions

Concentration-depletion zones around growing protein crystals (ferritin and lysozyme) were studied for the first time under reduced gravity conditions. These depletion zones, ideally having radial symmetry, are distorted by crystal and liquid movements during space protein crystal growth experiments as a consequence of buoyancy-driven convection triggered by residual accelerations and *g*-jitters. The ratio between the rate of crystal movement and that of bulk mass transport of growth units towards the surface of the growing

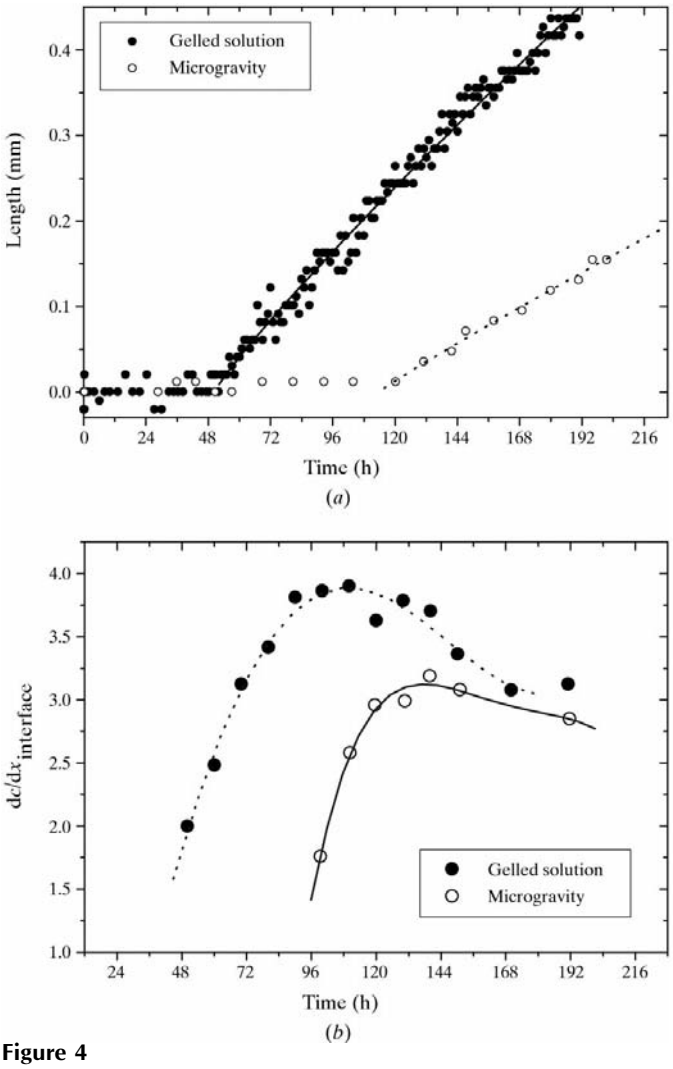

Figure 4
(*a*) Growth history of the seeded crystal surface as a function of time. The length is represented as the distance from the seed surface. The fitting function $y = A(x - B)^C$ included a cutoff term B indicating the beginning of growth ($A = 0.0054$, $B = 50.43628$, $C = 0.89421$ for the on-ground gelled experiment; $A = 0.00232$, $B = 113.82843$, $C = 0.94031$ for the space experiment). (*b*) Protein concentration gradients at the crystal surface as a function of the experimental time for the microgravity and on-ground experiments.

crystal is the key factor controlling the radial symmetry of the CDZ and hence the quality of the diffusive environment where crystals grow in microgravity experiments. The crystal growth rate and the concentration gradients observed seem to confirm that tetragonal lysozyme grows in the kinetic regime even when diffusive mass transport is ensured. The contribution of buoyancy-driven convection could be the source of the smaller supersaturation, supersaturation rate and concentration gradients observed in microgravity experiments with respect to gelled on-ground experiments.

Our results show that fluctuations in the gravity level as well as the actual average value of g during Space Shuttle missions need to be reduced in order to provide a desirable convection-free scenario for growing crystals in space experiments. The observed distortions of the diffusive environment in microgravity crystal growth must be taken into account when testing for crystal quality enhancements in space and when designing crystallization experiments in space as (i) the ratio between diffusive transport and surface-attachment kinetics could invalidate the positive effect of diffusive transport in microgravity and (ii) the maximum level of acceleration acceptable before destroying the benefits of microgravity experiments is a function of the protein diffusivity, solution viscosity and density, and the crystal density.

We acknowledge financial support from CICYT (Proyect ESP98-1347) and Consejo Superior de Investigaciones Científicas (CSIC). This work has been possible thanks to the APCF flight opportunity provided by the European Space Agency. We would like to thank Dornier GmbH for their help with APCF reactors and vibration tests during the preparation of experiment 2, the SAMS team for kindly providing us the accelerometric record of mission STS-95 and Professor Alex Chernov for useful discussion.

References

Boggon, T. J., Chayen, N. E., Snell, E. H., Dong, J., Lautenschlager, P., Potthast, L., Siddons, D. P., Stojanov, V., Gordon, E., Thompson, A. W., Zagalsky, P. F., Bi, R.-C. & Helliwell, J. R. (1998). *Philos. Trans. R. Soc. London Ser. A*, **356**, 1045–1061.

Bosch, R., Lautenschlager, P., Potthast, L. & Stapelmann, J. (1992). *J. Cryst. Growth*, **122**, 310–316.

Chayen, N. E., Snell, E. H., Helliwell, J. R. & Zagalsky, P. F. (1997). *J. Cryst. Growth*, **171**, 219–225.

Chernov, A. A. (1984). *Modern Crystallography III. Crystal Growth.* Berlin: Springer–Verlag.

García-Ruiz, J. M. (1999). *Microgravity Sci. Technol.* **12**, 1–4.

García-Ruiz, J. M., Gavira, J. A., Otálora, F., Guasch, A. & Coll, M. (1998). *Mater. Res. Bull.* **33**, 1593–1598.

García-Ruiz, J. M. & Otálora, F. (1997). *J. Cryst. Growth*, **182**, 155–167.

García-Ruiz, J. M., Otálora, F., Novella, M. L., Gavira, J. A., Sauter, C. & Vidal, O. (2001). In the press.

Hempstead, P. D., Yewdall, S. J., Fernie, A. R., Lawson, D. M., Artymiuk, P. J., Rice, D. W., Ford, G. C. & Harrison, P. M. (1997). *J. Mol. Biol.* **268**, 424–448.

Kam, Z., Shore, H. B. & Feher, G. (1978). *J. Mol. Biol.* **123**, 539–555.

Komatsu, H., Miyashita, S. & Suzuki, Y. (1993). *Jpn J. Appl. Phys.* **32**, L1855–L1857.

McPherson, A., Malkin, A. J., Kuznetsov, Y. G., Koszelak, S., Wells, M., Jenkins, G., Howard, J. & Lawson, G. (1999). *J. Cryst. Growth*, **196**, 572–586.

Maruyama, S., Shibata, T. & Tsukamoto, K. (1999). *Exp. Therm. Fluid Sci.* **19**, 34–48.

Miyashita, S., Komatsu, H., Suzuki, Y. & Nakada, T. (1994). *J. Cryst. Growth*, **141**, 419–424.

Molenkamp, T., Janssen, L. P. B. M. & Drenth, J. (1994). *Eur. Space Agency SP-1132*, **4**, 22–43.

Otálora, F. & García-Ruiz, J. M. (1997). *J. Cryst. Growth*, **182**, 141–154.

Pernodet, N., Maaloum, M. & Tinland, B. (1997). *Electrophoresis*, **18**, 55–58.

Petsev, D. N., Thomas, B. R., Yau, S.-T. & Vekilov, P. G. (2000). *Biophys. J.* **78**, 2060–2069.

Riès-Kautt, M., Broutin, I., Ducruix, A., Shepard, W., Kahn, R., Chayen, N., Blow, D., Paal, K., Littke, W., Lorber, B., Théobald-Dietrich, A. & Giegé, R. (1997). *J. Cryst. Growth*, **181**, 79–96.

Savino, R. & Monti, R. (1996). *J. Cryst. Growth*, **165**, 308–318.

Snell, E. H., Boggon, T. J., Helliwell, J. R., Moskowitz, M. E. & Nadarajah, A. (1997). *Acta Cryst.* D**53**, 747–755.

Snell, E. H., Helliwell, J. R., Boggon, T. J., Lautenschlager, P. & Potthast, L. (1996). *Acta Cryst.* D**52**, 529–533.

Tsukamoto, K., Yokoyama, E., Maruyama, S., Maiwa, K., Shimizu, K., Sekerka, R. F., Morita, T. & Yoda, S. (1998). *J. Jpn Soc. Microgravity Appl.* **15**, 2–9.

Walter, H. U. (1987). Editor. *Fluid Sciences and Materials Science in Space.* Berlin: Springer–Verlag.

Wang, M., Yin, X. B., Vekilov, P. G., Peng, R. W. & Ming, N. B. (1999). *Phys. Rev. E*, **60**, 1901-1905.